Dynamics of Cubic and Vibro-Impact Nonlinear Energy Sink: Analytical, Numerical, and Experimental Analysis

Tao Li, Sébastien Seguy, Alain Berlioz

Dynamics of cubic and vibro-impact Nonlinear Energy Sink (NES): analytical, numerical and experimental analysis

Tao Li
Université de Toulouse
ICA (Institut Clément Ader), CNRS,
INSA, ISAE, UPS, Mines Albi,
3 rue Caroline Aigle
F-31077, Toulouse, FRANCE
e-mail: tli@insa-toulouse.fr

Sébastien Seguy
Université de Toulouse
ICA (Institut Clément Ader), CNRS,
INSA, ISAE, UPS, Mines Albi,
3 rue Caroline Aigle
F-31077, Toulouse, FRANCE
e-mail: seguy@insa-toulouse.fr

Alain Berlioz
Université de Toulouse
ICA (Institut Clément Ader), CNRS,
INSA, ISAE, UPS, Mines Albi,
3 rue Caroline Aigle
F-31077, Toulouse, FRANCE
e-mail: alain.berlioz@univ-tlse3.fr

ABSTRACT

This paper is devoted to study and compare dynamics of primary Linear Oscillator (LO) coupled to cubic and Vibro-Impact (VI) Nonlinear Energy Sink (NES) under transient and periodic forcing. The classic analytical procedure combining the approach of invariant manifold and multiple scales is extended from the analysis of steady-state resonance to other regimes, especially Strongly Modulated Response (SMR). A general equation governing the variation of motion along the Slow Invariant Manifold (SIM) is obtained. Numerical results show its convenience to explain the transition from steady-state response to SMR and the characteristics of SMR for periodic forcing. Targeted energy transfer under transient forcing can also be well understood. Experimental results from LO coupled to VI NES under periodic forcing confirm the existence of SMR and its properties (e.g. chaotic). They also verify the feasibility of the general equation to explain complicated case like SMR in experiments.

1 Introduction

Nonlinear Energy Sink (NES) is a small attachment fixed to primary system with essential nonlinearity. It is proved that it can lead to irreversible energy transfer from primary system to NES and rapid dissipation of this localized energy. This phenomenon is called non-linear energy pumping or passive Targeted Energy Transfer (TET) which has been extensively studied during the last fifteen years [1, 2].

The initial studies of NES are concentrated on a NES with cubic nonlinearity. In the first two papers dedicated to study the dynamics of TET [3, 4], the NES is supposed with cubic nonlinearity which can be realized with two strings with pretensions. However, NES can possess other forms of nonlinearity. NES with general non-polynomial nonlinearity is studied in [5]. NES with piecewise nonlinearity is analyzed in [6]. For seismic mitigation, a Vibro-Impact (VI) NES is studied numerically and experimentally in [7,8]. It is realized though combining linear spring and vibro-impact elements and studied further in [9]. A simpler model of VI NES is presented in [10] and the VI NES is realized by a mass which can move freely in a cavity of the primary system and impact the system in two sides. The study of VI NES is extended from transient forcing to periodic forcing with experimental validation in [11]. It is also studied analytically and numerically under periodic forcing in [12]. It is also demonstrated that a simple eccentric rotator can be used as NES [13,14]. In addition, a NES realized with a nonlinear membrane in acoustic system is studied in [15,16] and multiple NESs in parallel are investigated in [17,18].

A classic analytical method combining the approach of invariant manifold and the multiple scales is introduced to the study of cubic NES in [19]. This method is generalized to NES with non-polynomial nonlinearity in [5], which is illustrated by two examples involving softening (non-polynomial) and piecewise-linear (non-analytic).

In the series of paper [10, 12, 20, 21], SIM is obtained with the above method and proved to be a good tool to describe the quantitative relation between primary system and NES. Moreover, it represents the set of all possible fixed points under 1:1 resonance and its topologic structure can be used to judge the existence of TET and SMR. Recently, it is founded that the topological structure of SIM is different for NES with piece-wise nonlinearity [6], cubic NES [22] and VI NES [11]. In [12], the authors assume that the special structure of SIM is the cause of the unique SMR for VI NES and it is named as chaotic SMR. In this same paper, this phenomenon is also claimed to exist for a rotational NES [13, 14]. However, this method is limited at the condition of 1:1 resonance. Moreover, although the existence of SMR can be judged from the structure of SIM obtained through this method, the actual variation of SMR cannot be explained further by it.

In one side, whether there exists one better analytical method to overcome the limit of the hypothesis (i.e. 1:1 resonance) to explain all possible SMRs of different NESs mentioned above or even more complicated regimes. In another side, whether this new or improved method can explain the more complicated results during the application of NES, for example, the complicated results during the application of VI NES to quench the chatter instability in turning process [23].

In this paper, the LO separately coupled to cubic NES and VI NES is studied. The structure is as follows: Section 2 is devoted to the analytical treatment of the governing equation of motion. Section 3, numerical results is used to verify analytical developments. In the next section, experimental results are demonstrated. Finally, concluding remarks are addressed.

2 Theoretic Developements

A Linear Oscillator (LO) coupled to cubic NES and VI NES separately is studied under transient and periodic forcing respectively. The objective is to get the SIM when LO and NES are in 1:1 resonance. The theoretic developments presented herein are based on the method used in [22] for cubic NES and [11] for VI NES.

2.1 Cubic NES

System of harmonically forced LO attached with cubic NES presented in Fig. 1 is described by the following equation of motion:

$$\begin{aligned} &\ddot{x}+\varepsilon\lambda_1\dot{x}+x+\varepsilon\lambda_2(\dot{x}-\dot{y})+\varepsilon K(x-y)^3 \\ &\quad=\varepsilon G\sin\Omega\tau+\varepsilon^2\lambda_1 G\Omega\cos\Omega\tau \\ &\varepsilon\ddot{y}+\varepsilon\lambda_2(\dot{y}-\dot{x})+\varepsilon K(y-x)^3=0 \end{aligned} \tag{1}$$

The corresponding physical parameters are expressed as follows:

$$\varepsilon=\frac{m_2}{m_1},\quad {\omega_0}^2=\frac{k_1}{m_1},\quad K=\frac{k_2}{m_2{\omega_0}^2},\quad \lambda_1=\frac{c_1}{m_2\omega_0},$$
$$\lambda_2=\frac{c_2}{m_2\omega_0},\quad G=\frac{F}{\varepsilon},\quad \Omega=\frac{\omega}{\omega_0},\quad \tau=\omega_0 t$$

where x, m_1, c_1, k_1 and y, m_2, c_2, k_2 are the displacement, mass, damping and stiffness of the LO and the cubic NES respectively, the dots denote differentiation with respect to τ.

[Fig. 1 about here.]

New variables representing the displacement of the center of mass and the internal displacement of the cubic NES are introduced as follows:

$$v=x+\varepsilon y,\quad w=x-y \tag{2}$$

Substituting Eq. (2) into Eqs. (1):

$$\begin{aligned}
&\ddot{v}+\varepsilon\lambda_1\frac{\dot{v}+\varepsilon\dot{w}}{1+\varepsilon}+\frac{v+\varepsilon w}{1+\varepsilon}=\varepsilon G\sin\Omega\tau+\varepsilon^2\lambda_1 G\Omega\cos\Omega\tau\\
&\ddot{w}+\varepsilon\lambda_1\frac{\dot{v}+\varepsilon\dot{w}}{1+\varepsilon}+\frac{v+\varepsilon w}{1+\varepsilon}+\lambda_2(1+\varepsilon)\dot{w}+K(1+\varepsilon)w^3\\
&\qquad=\varepsilon G\sin\Omega t+\varepsilon^2\lambda_1 G\Omega\cos\Omega t
\end{aligned}\tag{3}$$

In the context of energy pumping, the mass ratio ε is supposed to be small ($\approx 1\%$). In this case, Eq. (3) may be analyzed by multiple scales method with respect to this small parameter. Multiple scales are introduced in the following form:

$$\begin{aligned}
v(\tau;\varepsilon)&=v_0(\tau_0,\tau_1,\ldots)+\varepsilon v_1(\tau_0,\tau_1,\ldots)+\ldots,\\
w(\tau;\varepsilon)&=w_0(\tau_0,\tau_1,\ldots)+\varepsilon w_1(\tau_0,\tau_1,\ldots)+\ldots,\\
\tau_k&=\varepsilon^k\tau,\quad k=0,1,\ldots
\end{aligned}\tag{4}$$

A detuning parameter σ representing the nearness of the forcing frequency Ω to the reduced natural frequency of the LO is introduced:

$$\Omega=1+\varepsilon\sigma\tag{5}$$

Substituting Eqs. (4) and (5) into Eqs. (3) and equating coefficients of ε^0 and ε^1:

$$\begin{aligned}
&\varepsilon^0:\\
&\quad\frac{\partial^2}{\partial{\tau_0}^2}v_0+v_0=0\\
&\quad\frac{\partial^2}{\partial{\tau_0}^2}w_0+\lambda_2\frac{\partial}{\partial\tau_0}w_0+v_0+Kw_0^3=0
\end{aligned}\tag{6}$$

ε^1 :

$$\frac{\partial^2}{\partial\tau_0{}^2}v_1 + v_1 = -2\frac{\partial^2}{\partial\tau_0\partial\tau_1}v_0 - \lambda_1\frac{\partial}{\partial\tau_0}v_0 + v_0 + F\cos(\Omega\tau_0) - w_0 \tag{7}$$

The following complex variables are introduced under supposition of 1:1 resonance to obtain SIM:

$$\begin{aligned} v_0 &= 1/2A(\tau_1)\,e^{i\tau_0} + 1/2\overline{A}(\tau_1)\,e^{-i\tau_0} \\ A(\tau_1) &= N_1(\tau_1)\,e^{i\theta_1(\tau_1)} \\ w_0 &= 1/2B(\tau_1)\,e^{i\tau_0} + 1/2\overline{B}(\tau_1)\,e^{-i\tau_0} \\ B(\tau_1) &= N_2(\tau_1)\,e^{i\theta_2(\tau_1)} \end{aligned} \tag{8}$$

Substituting Eq. (8) into Eqs. (6) and the equation of the SIM presented in Fig. 2 can be obtained. As to the stability, the analysis is already developed in [20].

$$\begin{aligned} {N_1}^2 &= \left(1 + {\lambda_2}^2\right)Z - \frac{3K}{2}Z^2 + \frac{9K^2}{16}Z^3 \\ Z &= {N_2}^2 \end{aligned} \tag{9}$$

[Fig. 2 about here.]

Concerning the study of non 1:1 resonance (SMR), the following formula is introduced, among which the component of w containing the same frequency with the LO (frequency of outside forcing for periodic forcing or natural frequency of LO for transient forcing) can be developed in Fourier series and is supposed in the following form:

$$\begin{aligned} w_0 &= 1/2E(\tau_1)\,e^{i\tau_0} + 1/2\overline{E}(\tau_1)\,e^{-i\tau_0} \\ &+ 1/2A(\tau_1)\,e^{i\tau_0} + 1/2\overline{A}(\tau_1)\,e^{-i\tau_0} + RFC \\ E(\tau_1) &= N_3(\tau_1)\,e^{i\theta_3(\tau_1)} \end{aligned} \tag{10}$$

where RFC represents the rest frequency components and $E(\tau_1)$ is directly decided by the motion of cubic NES.

Substituting the first two equations of Eqs. (8) and Eqs. (10) into the first equation of (7) and eliminating the secular terms, the following equation governing the variation of the slow variation of LO with respect to τ_1 can be obtained:

$$\frac{d}{d\tau_1}N_1 = -\frac{1}{2}\lambda_1 N_1 - \frac{1}{2}N_3 \sin(\Theta) + \frac{1}{2}G\sin(\eta) \tag{11}$$

where

$$\begin{aligned} \Theta &= \theta_3 - \theta_1 \\ \eta &= \tau_1\sigma - \theta_1 \end{aligned} \tag{12}$$

Θ represents the phase difference between relative displacement and that of LO. η represents the phase difference between outside forcing and motion of LO.

2.2 VI NES

System of harmonically forced LO attached with VI NES presented in Fig. 3 is described by the following equations:

$$\begin{aligned} &\ddot{x} + \varepsilon\lambda_1\dot{x} + x = \varepsilon G\sin\Omega\tau + \varepsilon^2\lambda_1 G\Omega\cos\Omega\tau \\ &\varepsilon\ddot{y} = 0 \\ &\forall\,|x-y| < b \end{aligned} \tag{13}$$

where

$$\begin{aligned} \varepsilon = \frac{m_2}{m_1}, \quad {\omega_0}^2 = \frac{k_1}{m_1}, \quad \tau = \omega_0 t, \\ \lambda_1 = \frac{c_1}{m_2\omega_0}, \quad \Omega = \frac{\omega}{\omega_0}, \quad G = \frac{F}{\varepsilon} \end{aligned}$$

[Fig. 3 about here.]

The meaning of notations is the same as that for system with Cubic NES and b represents a parameter related to the length of cavity.

When $|x-y|=b$, a impact occurs. The state of the system after impact is obtained using the simplified shock theory and the condition of total momentum conservation:

$$\begin{gathered} x^{+}=x^{-}, \quad y^{+}=y^{-} \\ \dot{x}^{+}+\varepsilon\dot{y}^{+}=\dot{x}^{-}+\varepsilon\dot{y}^{-}, \quad \dot{x}^{+}-\dot{y}^{+}=-r\left(\dot{x}^{-}-\dot{y}^{-}\right), \\ \text{for } |x-y|=b \end{gathered} \tag{14}$$

where r is the restitution coefficient of impact and the superscripts $+$ and $-$ denotes time immediately after and before impact. New variables representing the displacement of the center of mass and the internal displacement of the VI NES are introduced as follows:

$$v=x+\varepsilon y, \quad w=x-y \tag{15}$$

Substituting Eq. (15) into Eqs. (13) and (14), the equation between impact in barycentric coordinate are given as:

$$\begin{gathered} \ddot{v}+\varepsilon\lambda_1\frac{\dot{v}+\varepsilon\dot{w}}{1+\varepsilon}+\frac{v+\varepsilon w}{1+\varepsilon}=\varepsilon G\sin\Omega\tau+\varepsilon^2\lambda_1 G\Omega\cos\Omega\tau \\ \ddot{w}+\varepsilon\lambda_1\frac{\dot{v}+\varepsilon\dot{w}}{1+\varepsilon}+\frac{v+\varepsilon w}{1+\varepsilon}=\varepsilon G\sin\Omega\tau+\varepsilon^2\lambda_1 G\Omega\cos\Omega\tau \\ \forall |w|<b \end{gathered} \tag{16}$$

And the impact condition (14) is rewritten as:

$$\begin{gathered} v^{+}=v^{-}, \quad w^{+}=w^{-}, \\ \dot{v}^{+}=\dot{v}^{-}, \quad \dot{w}^{+}=-r\dot{w}^{-}, \quad \text{for } |w|=b \end{gathered} \tag{17}$$

Multiple scales are introduced in the following form:

$$
\begin{aligned}
v(\tau;\varepsilon) &= v_0(\tau_0,\tau_1,\ldots)+\varepsilon v_1(\tau_0,\tau_1,\ldots)+\ldots,\\
w(\tau;\varepsilon) &= w_0(\tau_0,\tau_1,\ldots)+\varepsilon w_1(\tau_0,\tau_1,\ldots)+\ldots\\
\tau_k &= \varepsilon^k\tau, \quad k=0,1,\ldots
\end{aligned}
\tag{18}
$$

A detuning parameter (σ) representing the nearness of the forcing frequency Ω to the reduced natural frequency of the LO is introduced:

$$
\Omega = 1+\varepsilon\sigma \tag{19}
$$

Substituting Eqs. (18) and (19) into Eqs. (16), (17) and equating coefficients of like power of ε gives:

Order ε^0:

$$
\begin{aligned}
D_0^2 v_0 + v_0 &= 0\\
D_0^2 w_0 + v_0 &= 0, \quad \forall |w_0| < b
\end{aligned}
\tag{20}
$$

$$
\begin{aligned}
v_0^+ &= v_0^-, \quad w_0^+ = w_0^-,\\
D_0 v_0^+ &= D_0 v_0^-, \quad D_0 w_0^+ = -rD_0 w_0^-, \quad \text{for } |w_0| = b
\end{aligned}
\tag{21}
$$

Order ε^1:

$$
\begin{aligned}
D_0^2 v_1 + v_1 = &-2D_0D_1v_0 - \lambda_1 D_0 v_0 - w_0 + v_0\\
&+G\sin(\tau_0+\sigma\tau_1)
\end{aligned}
\tag{22}
$$

Here, the SIM will be obtained through the first order and the fixed points will be obtained by combining the first order and the second order as what have been done for cubic NES.

The first equation of system (20), taking into account Eq. (21) simply represents an undamped harmonic oscillator and its solution can be expressed as follow:

$$v_0 = C(\tau_1)\sin(\tau_0 + \theta(\tau_1)) \tag{23}$$

The second equation of system (20) with (21) represents an harmonically forced impact oscillator with symmetric barrier. Under the assumption of $1:1$ resonance (i.e. motion with two symmetric impact per cycle), its solution can be searched in the following form:

$$w_0 = C(\tau_1)\sin(\tau_0 + \theta(\tau_1)) + \frac{2}{\pi}B(\tau_1)\Pi(\tau_0 + \eta(\tau_1)) \tag{24}$$

Where $\Pi(z)$ is a non-smooth zig-zag function [24]. This folded function and its derivative is depicted in Fig. 4 and are expressed as follows:

$$\Pi(z) = \arcsin(\sin z), \quad M(z) = \frac{d\Pi}{dz} = sgn(\cos z) \tag{25}$$

[Fig. 4 about here.]

According to Eq. (24) and (25), impact occurs at $T_0 = \pi/2 - \eta + j\pi$ with $j = 0, 1, 2, \ldots$. The impact condition $|w_0| = b$ is rewritten with Eq. (24) as:

$$C\cos(\eta - \theta) = b - B \tag{26}$$

Rewriting now the inelastic impact condition (21) yields:

$$C(1+r)\sin(\eta - \theta) = \frac{2}{\pi}B(1-r) \tag{27}$$

Combining Eqs. (26) and (27), a relation between the slow variables B and C presented in Fig. 5 is obtained as follow:

$$C^2 = \left(1 + \frac{4(1-r)^2}{\pi^2(1+r)^2}\right) B^2 - 2bB + b^2 \tag{28}$$

[Fig. 5 about here.]

The analysis of the stability is fully developed in [25].

In order to obtain the fixed points or study the evolution of the system on the SIM for SMR, Eq. (22) at the next order of approximation is analyzed. To identify terms that produce secular terms, the function of w_0 is expanded in Fourier series in the following way:

$$w_0 = C(\tau_1)\sin(\tau_0 + \theta(\tau_1)) + E(\tau_1)\sin(\tau_0 + \zeta(T_1)) + RFC \tag{29}$$

where RFC represents the rest frequency components. $E(\tau_1)$ is decided by the motion of VI NES.

Substituting Eq. (23), (24) and (29) into Eq. (22) and eliminating terms that produce secular terms gives:

$$D_1 C = -\tfrac{1}{2}\lambda_1 C - \tfrac{1}{2}E\sin(\Theta) + \tfrac{1}{2}G\sin(\eta) \tag{30}$$

where

$$\begin{aligned} \Theta &= \zeta - \theta \\ \eta &= \sigma\tau_1 - \theta \end{aligned} \tag{31}$$

Θ and η have the same meaning as defined in Eq. (12).

2.3 Remarks

A general governing equation of motion is obtained, specifically Eq. (11) for cubic NES and Eq. (30) for VI NES. Therefore, although the topological structure of SIM is different, the underlying governing equation of motion in the slow time scale is the same. In another word, though the specific variation of motion for NES described by SIM is different, the

Fourier series development for NES and its variation may have some similarities showed in the general governing equation.

In short, the classic method is extended by relaxing the condition of 1:1 resonance. It can be used to explain the variation of complicated response (e.g. SMR) in which the variation of motion (LO and NES) is not steady.

In this way, the first order (e.i. ε^0) can be used to obtain SIM which represents the set of fixed points for all possible initial conditions and parameters. The second order (e.i. ε^1) is used to get slower invariant manifold and combined with the first order to obtain fixed points for specific parameters and conditions.

3 Numerical Analysis

In this part, the objective is to show the important role of SIM to control the variation of motion of system under transient and periodic forcing by numerical simulations, based on which some critical characteristics of SMR can be detected and explained by the general governing equation obtained in the last part.

The simulations will be based on the same LO coupled to cubic and VI NES separately under transient ($G = 0$) and periodic ($G \neq 0$) forcing with the following fixed parameters: $\lambda_1 = 1.43, \varepsilon = 0.84\%$ for cubic and VI NES, $\lambda_2 = 0.13$ for cubic NES.

It has to be pointed out that $v \approx x$ considering $v = x + \varepsilon y$ with $\varepsilon = 0.84\%$ in the following analysis.

3.1 Numerical Results for Cubic NES

The simulation will be based on the Eq. (3). **For transient forcing**, different types of response can exist by varying the parameters. Herein, just the regime (TET excited) is showed in Fig. 6. The history of response can be categorized into two parts, that is A and B showed in Fig. 6 (a). The TET is excited in the part A, during which the displacement of x decreases with an almost linear slope and the amplitude of cubic NES is much bigger than that in the unexcited part B as showed in Fig. 6 (b). In Fig. 6 (d), the motion of system is projected to SIM and it can predict the motion in the part A as well. However, it cannot predict the part B with escape from the 1:1 resonance.

[Fig. 6 about here.]

The above phenomena can be clearly explained by Eq. (11). During the whole process, the value of outside force is zero. For part A, the decrease of N_1 (amplitude of v) at the slow time scale is decided by the value of N_3 (large amplitude of cubic NES) and the slope is almost straight because of almost constant value of N_3. In part B, the value of N_3 becomes very small, N_1 (i.e. damping) plays the main role for its reduction.

For periodic forcing, just the results of SMR are demonstrated in Figs. 7 and 8 .

The response can be categorized into two parts (A and B) according to the increase and decrease of the amplitude of v showed in Fig. 7(a) . In the part A, the amplitude of y and w is small compared to that in the part B demonstrated respectively in Fig. 7(b) and (c). In Fig. 7(d), the part A is divided into three small parts. For sub-part A2, 1:1 resonance exists and the value of y is still small. For parts A1 and A3, there do not exist 1:1 resonance. Globally, the SIM predicts the 1:1 resonance parts A2 and B well.

[Fig. 7 about here.]

[Fig. 8 about here.]

More detailed characteristics (e.g. frequency and amplitude) can be obtained in the frequency domain by using the Hilbert Transform (HT) and Wavelet Transform (WT) function in Matlab [26]. The result is showed in Fig. 8. Specifically, the envelope of v and y is showed in Fig. 8(a), through which the value change of v and y is clearly demonstrated. In Fig. 8(b), two intervals of 1:1 transient resonance capture (TRC) is clearly observed by almost fixed phase difference between v and y and they are interrupted by escape of resonance. In Fig. 8(c)(d)(e)(f), the 1:1 resonance part of the same frequency between v and y is clearly illustrated and the resonance frequency is showed by the red dotted line.

It is difficult to explain SMR as stated in [20], especially about the parts connecting these TRCs in which the hypothesis 1:1 resonance does not hold. With the general governing Eq. (11) developed in the former part, all parts can be explained to some extent. For part B, the left part Eq. (11) will be less than zero because of large value of N_3 and fixed phase difference which means the decrease of amplitude of LO in the slow time scale. For part A, the small value of N_3 with varying phase difference will result in the positive value of left part of Eq. (11) that leads to the increase of amplitude of LO, in which the outside force plays the main role.

3.2 Numerical Results for VI NES

Numerical simulations for VI NES are based on Eqs. (13) and (14). The b related to the length of cavity is varied to detect different regimes.

For transient forcing, different regimes are observed. One typical response with TET activated is showed in Fig. 9. The difference for VI NES from cubic NES is that the former is piece-wise. However, the similar two parts are observed and can be explained by the general governing Eq. (30) as have been done for cubic NES.

[Fig. 9 about here.]

For periodic forcing, just a SMR similar to that of cubic NES is showed in Fig. 10. It is studied in detail in [25] and is named as chaotic SMR in [12]. It is seen that the local maximum value is different every time in Fig. 10(a) and Fig. 11(a), which is different from that of cubic NES. The 1:1 resonance can be observed from the phase difference between v and y demonstrated in Fig. 11(b). Moreover, the slow variation of the phase difference shows the move between different 1:1 resonance responses. In Fig. 11(c)(d), the frequency variation of v and y is obtained from HT by excluding the big noise that represents the impact moments.

Globally, the law of the variation for frequency and amplitude is similar to these of cubic NES, therefore it is can be explained in the same way.

[Fig. 10 about here.]

[Fig. 11 about here.]

3.3 Remarks

The general governing equation is used to explain the non 1:1 resonance for both cubic NES and VI NES, specifically the case under transient forcing and the SMR under periodic forcing. The above analysis process demonstrates its facility to understand the variation of non 1:1 resonance for numerical results. In the next part, its ability to explain the experimental results will be showed.

4 Experimental verifications

[Table 1 about here.]

The experimental setup is presented in Fig. 12(b). It consists of a LO, with an embedded VI NES. The whole system is embedded on $10kN$ electrodynamic shaker. The displacement of the LO as well as the imposed displacement of the shaker are measured using contact-less laser displacement sensors. The acceleration of the LO is mearsured by a accelerometer. A detailed view of the VI NES is presented in Fig. 12(a). It simply consists of a closed cavity of length $d+2b$, where d is the diameter of the ball. Each cover is made of hardened steel. The parameters of the system have been identified by performing modal analysis and are summarized in Table 1.

[Fig. 12 about here.]

A chaotic SMR about VI NES is showed in Fig. 13. The forcing amplitude is fixed to 0.423mm and the forcing frequency is fixed to 8Hz. The blue line in Fig. 13(a) represents the acceleration of LO and the green cross dots represent the times and the values of the impact moments. It is seen that the LO and VI NES are in 1:1 resonance by two impacts during one period of LO except some intervals with no impact during one period of LO, specifically the intervals around t and $t \in \{0.4s, 2.4s, 4.7s\}$. Another phenomenon is that the value of the acceleration in the impact moment for 1:1 resonance change continuously.

[Fig. 13 about here.]

In Fig. 13(b), the displacement of LO, the acceleration of LO and the displacement of forcing are superimposed. One enlarged view of Fig. 13(b) is showed in Fig. 13(c). It is observed that the displacement of LO increases and decreases alternatively rather than remains constant. An enlarged view shows that if the value of acceleration is big enough, it will decrease, or it will increase when there is not enough number of impacts or the value of acceleration in the impact moment is not big enough.

In Eq. (30), the value of G in Eq. (30) is directly related to that of acceleration in the impact moment and the density of impact. The amplitude of LO will change according to that of G. This equation can explain the above experimental phenomenon well.

5 Conclusion

This paper is dedicated to generalize the classic analytical method to better understand the non 1:1 resonance response regimes from numerical study and the complicated experimental results. Firstly, a general analytical method extended from classic method is obtained through relaxing the condition of 1:1 resonance and it is applied to cubic and VI NES. Then the developed analytical method is used to explain the excited TET under transient forcing and the SMR under periodic forcing for these two NES. Finally, a chaotic SMR from the experimental results is used to demonstrate the feasibility of the general analytical method.

A general governing equation of motion is obtained and its ability to explain the non 1:1 resonance is demonstrated by two examples in numerical study, namely excited TET in transient case and the SMR in the periodic case. Its facility applied to the complicated experimental results is validated by its ability to explain the SMR detected in experiments.

In addition, the experimental results confirm the existence of the SMR encountered for VI NES and provide much more information than in [11]. The amplitude variation of LO and time variation of impact moment give experimental proof to chaotic properties of SMR defined in [12]. Moreover, since the 1:1 resonance is directly related to the TET, the experimental results show that VI NES is an ideal candidate to illustrate this characteristic. For VI NES, whether the system is in 1:1 resonance is judged from the impact directly rather than using waveform transform.

Although this method can extend the ability of classic analytical method, it still cannot obtain analytical results for the complicated regimes like SMR or experimental phenomena. For example, it could be known from this method that the case with more force in the moment of impact and 1:1 resonance between LO and VI NES is better, but how to ensure this by precise analytical calculation is still not clear.

Acknowledgements

The authors acknowledge the French Ministry of Science and the Chinese Scholarship Council under grant N° 201304490063 for their financial support.

Reference

[1] Lee, Y., Vakakis, A. F., Bergman, L., McFarland, D., Kerschen, G., Nucera, F., Tsakirtzis, S., and Panagopoulos, P., 2008. "Passive non-linear targeted energy transfer and its applications to vibration absorption: a review". *Proceedings of the Institution of Mechanical Engineers, Part K: Journal of Multi-body Dynamics,* **222**(2), pp. 77–134.

[2] Vakakis, A. F., Gendelman, O., Bergman, L., McFarland, D., Kerschen, G., and Lee, Y., 2008. *Nonlinear targeted energy transfer in mechanical and structural systems*, Vol. 156. Springer Science & Business Media.

[3] Gendelman, O., Manevitch, L., Vakakis, A., and M'Closkey, R., 2001. "Energy pumping in nonlinear mechanical oscillators: Part i: Dynamics of the underlying hamiltonian systems". *Journal of Applied Mechanics,* **68**(1), pp. 34–41.

[4] Vakakis, A., and Gendelman, O., 2001. "Energy pumping in nonlinear mechanical oscillators: Part ii: Resonance capture". *Journal of Applied Mechanics,* **68**(1), pp. 42–48.

[5] Gendelman, O. V., 2008. "Targeted energy transfer in systems with non-polynomial nonlinearity". *Journal of Sound and Vibration,* **315**(3), pp. 732–745.

[6] Lamarque, C., Gendelman, O., Ture Savadkoohi, A., and Etcheverria, E., 2011. "Targeted energy transfer in mechanical systems by means of non-smooth nonlinear energy sink". *Acta mechanica,* **221**(1), pp. 175–200.

[7] Nucera, F., Vakakis, A., McFarland, D., Bergman, L., and Kerschen, G., 2007. "Targeted energy transfers in vibro-impact oscillators for seismic mitigation". *Nonlinear Dynamics,* **50**(3), pp. 651–677.

[8] Nucera, F., Lo Iacono, F., McFarland, D., Bergman, L., and Vakakis, A., 2008. "Application of broadband nonlinear targeted energy transfers for seismic mitigation of a shear frame: Experimental results". *Journal of Sound and Vibration,* **313**(1), pp. 57–76.

[9] Lee, Y., Nucera, F., Vakakis, A., McFarland, D., and Bergman, L., 2009. "Periodic orbits, damped transitions and targeted energy transfers in oscillators with vibro-impact attachments". *Physica D: Nonlinear Phenomena,* **238**(18), pp. 1868–1896.

[10] Gendelman, O., 2012. "Analytic treatment of a system with a vibro-impact nonlinear energy sink". *Journal of Sound and Vibration,* **331**, pp. 4599–4608.

[11] Gourc, E., Michon, G., Seguy, S., and Berlioz, A., 2015. "Targeted energy transfer under harmonic forcing with a vibro-impact nonlinear energy sink: Analytical and experimental developments". *Journal of Vibration and Acoustics,* **137**(3), p. 031008.

[12] Gendelman, O., and Alloni, A., 2015. "Dynamics of forced system with vibro-impact energy sink". *Journal of Sound and Vibration,* **358**, pp. 301–314.

[13] Gendelman, O., Sigalov, G., Manevitch, L., Mane, M., Vakakis, A., and Bergman, L., 2012. "Dynamics of an eccentric rotational nonlinear energy sink". *Journal of applied mechanics,* **79**(1), p. 011012.

[14] Sigalov, G., Gendelman, O., Al-Shudeifat, M., Manevitch, L., Vakakis, A., and Bergman, L., 2012. "Resonance captures and targeted energy transfers in an inertially-coupled rotational nonlinear energy sink". *Nonlinear dynamics,* **69**(4), pp. 1693–1704.

[15] Cochelin, B., Herzog, P., and Mattei, P.-O., 2006. "Experimental evidence of energy pumping in acoustics". *Comptes Rendus Mécanique,* **334**(11), pp. 639–644.

[16] Bellet, R., Cochelin, B., Herzog, P., and Mattei, P.-O., 2010. "Experimental study of targeted energy transfer from an acoustic system to a nonlinear membrane absorber". *Journal of Sound and Vibration,* **329**(14), pp. 2768–2791.

[17] Vaurigaud, B., Savadkoohi, A. T., and Lamarque, C.-H., 2011. "Targeted energy transfer with parallel nonlinear energy sinks. part i: Design theory and numerical results". *Nonlinear dynamics,* **66**(4), pp. 763–780.

[18] Savadkoohi, A. T., Vaurigaud, B., Lamarque, C.-H., and Pernot, S., 2012. "Targeted energy transfer with parallel nonlinear energy sinks, part ii: theory and experiments". *Nonlinear dynamics,* **67**(1), pp. 37–46.

[19] Gendelman, O., 2004. "Bifurcations of nonlinear normal modes of linear oscillator with strongly nonlinear damped attachment". *Nonlinear Dynamics,* **37**(2), pp. 115–128.

[20] Gendelman, O., Starosvetsky, Y., and Feldman, M., 2008. "Attractors of harmonically forced linear oscillator with

attached nonlinear energy sink i: Description of response regimes". *Nonlinear Dynamics,* **51**(1-2), pp. 31–46.

[21] Starosvetsky, Y., and Gendelman, O., 2008. "Strongly modulated response in forced 2dof oscillatory system with essential mass and potential asymmetry". *Physica D: Nonlinear Phenomena,* **237**(13), pp. 1719–1733.

[22] Gourc, E., Michon, G., Seguy, S., and Berlioz, A., 2014. "Experimental investigation and design optimization of targeted energy transfer under periodic forcing". *Journal of Vibration and Acoustics,* **136**(2), p. 021021.

[23] Gourc, E., Seguy, S., Michon, G., Berlioz, A., and Mann, B., 2015. "Quenching chatter instability in turning process with a vibro-impact nonlinear energy sink". *Journal of Sound and Vibration,* **355**, pp. 392–406.

[24] Pilipchuk, V., 2002. "Some remarks on non-smooth transformations of space and time for vibrating systems with rigid barriers". *Journal of applied mathematics and mechanics,* **66**(1), pp. 31–37.

[25] Gourc, E., 2013. "Etude du contrôle passif par pompage énergétique sous sollicitation harmonique: Analyses théoriques et expérimentales". PhD thesis, Toulouse, INSA.

[26] Poularikas, A. D., 1998. *Handbook of formulas and tables for signal processing*, Vol. 13. CRC Press.

List of Tables

List of Figures

Table 1. Parameters of the experiment

Physical Parameters			
m_1	$4.168\,kg$	c_1	$3.02\,Ns/m$
k_1	$11.47*10^3\,N/m$	m_2	$32\,g$
b	$11.5\,mm$	r	0.6
Reduced Parameters			
ε	0.76%	λ	1.80

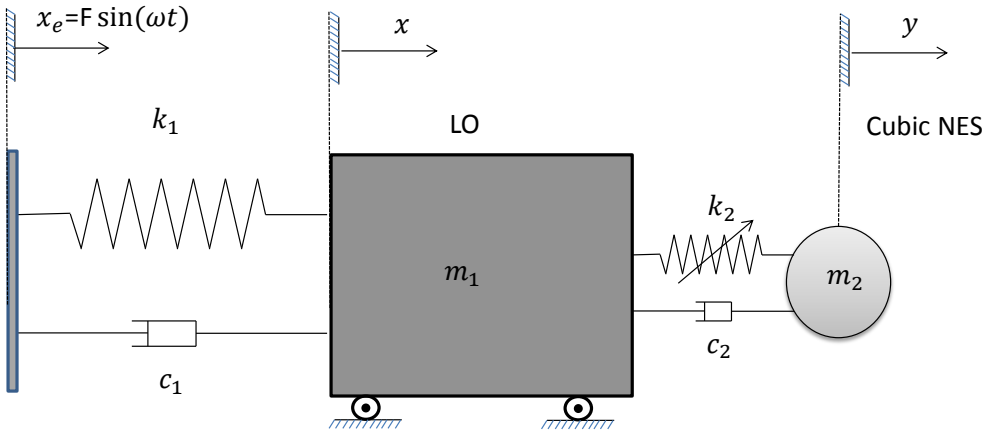

Fig. 1. Representation of the LO coupled to a cubic NES.

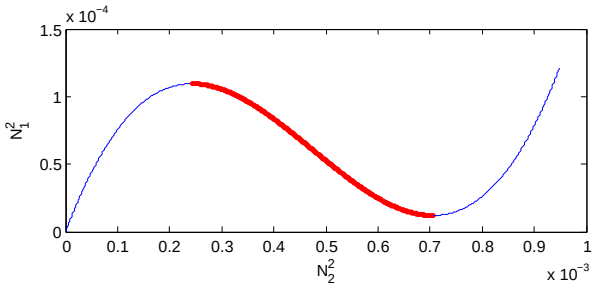

Fig. 2. SIM of cubic NES: two stable branches in blue thin line and one unstable branch in red thick line.

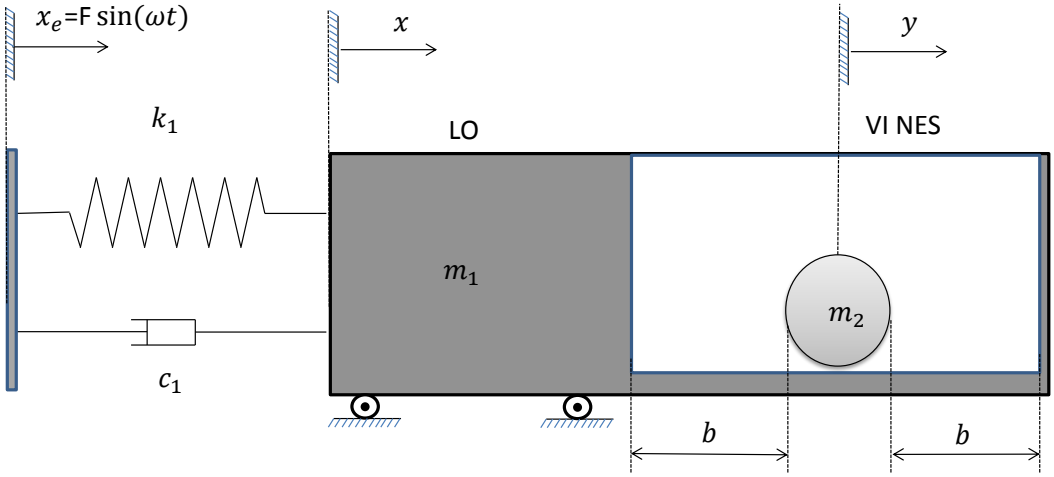

Fig. 3. Representation of the LO coupled to a VI NES.

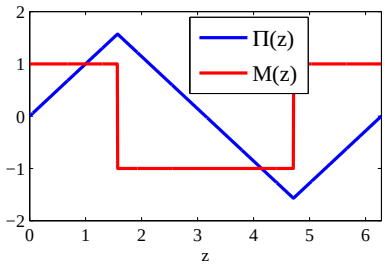

Fig. 4. Representation of the non-smooth functions $\Pi(z)$ and $M(z)$.

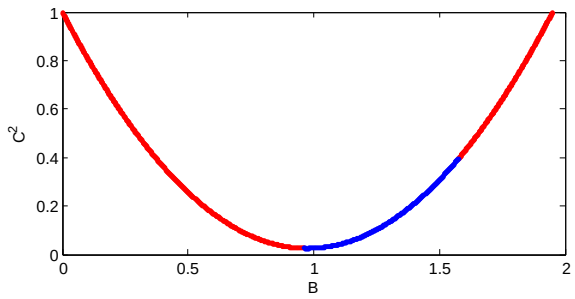

Fig. 5. SIM of VI NES: one stable branch in blue line and two unstable branches in red line.

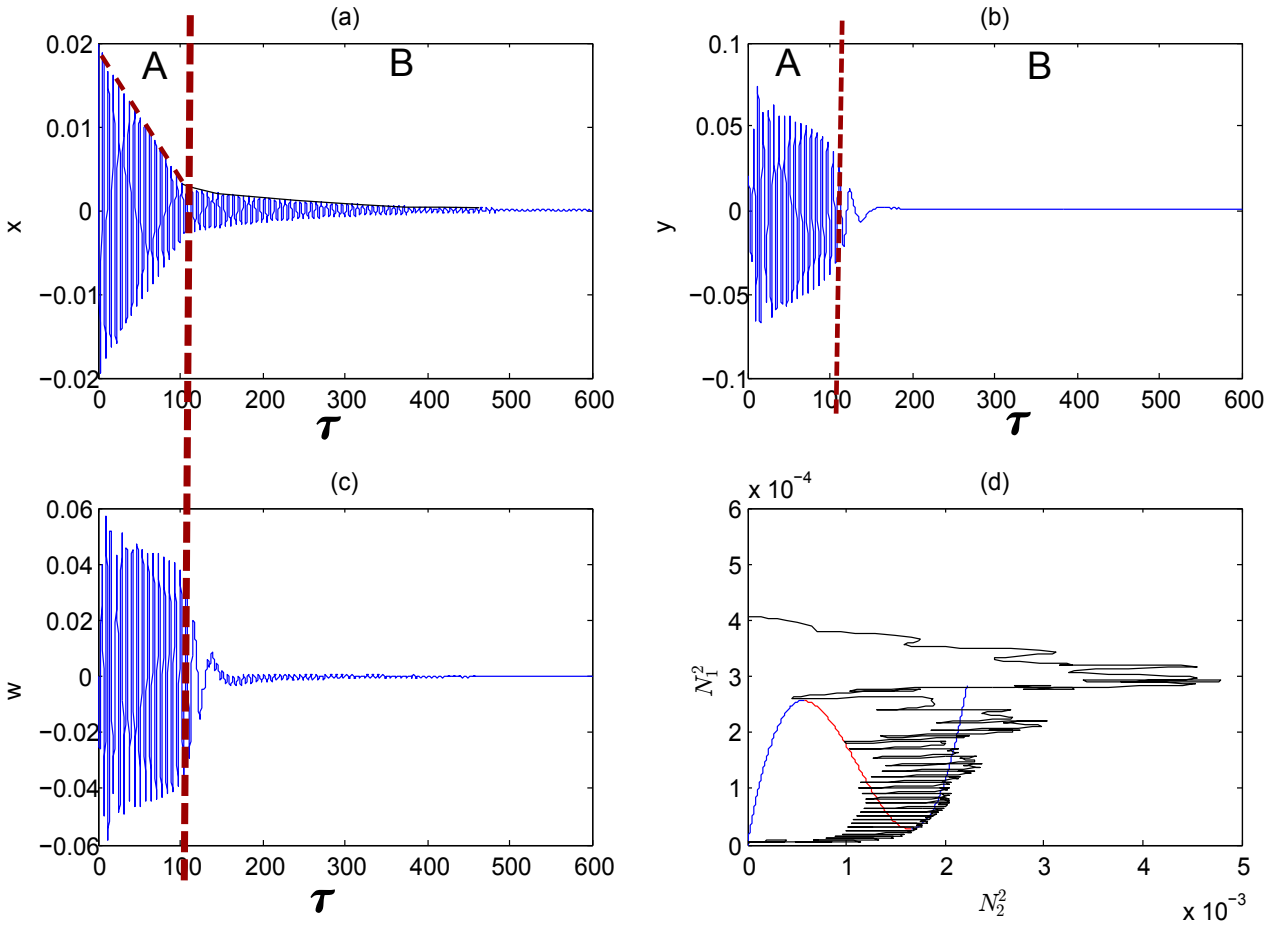

Fig. 6. Cubic NES under transient forcing with parameters $K = 800, G = 0$ and initial conditions $x_0 = 0.02, \dot{x_0} = 0, y_0 = 0, \dot{y_0} = 0$. (a) Displacement of LO with cubic NES. (b) Displacement of cubic NES. (c) Relative displacement between LO and cubic NES. (d) SIM and trace between LO and cubic NES: black curve represents projected motion.

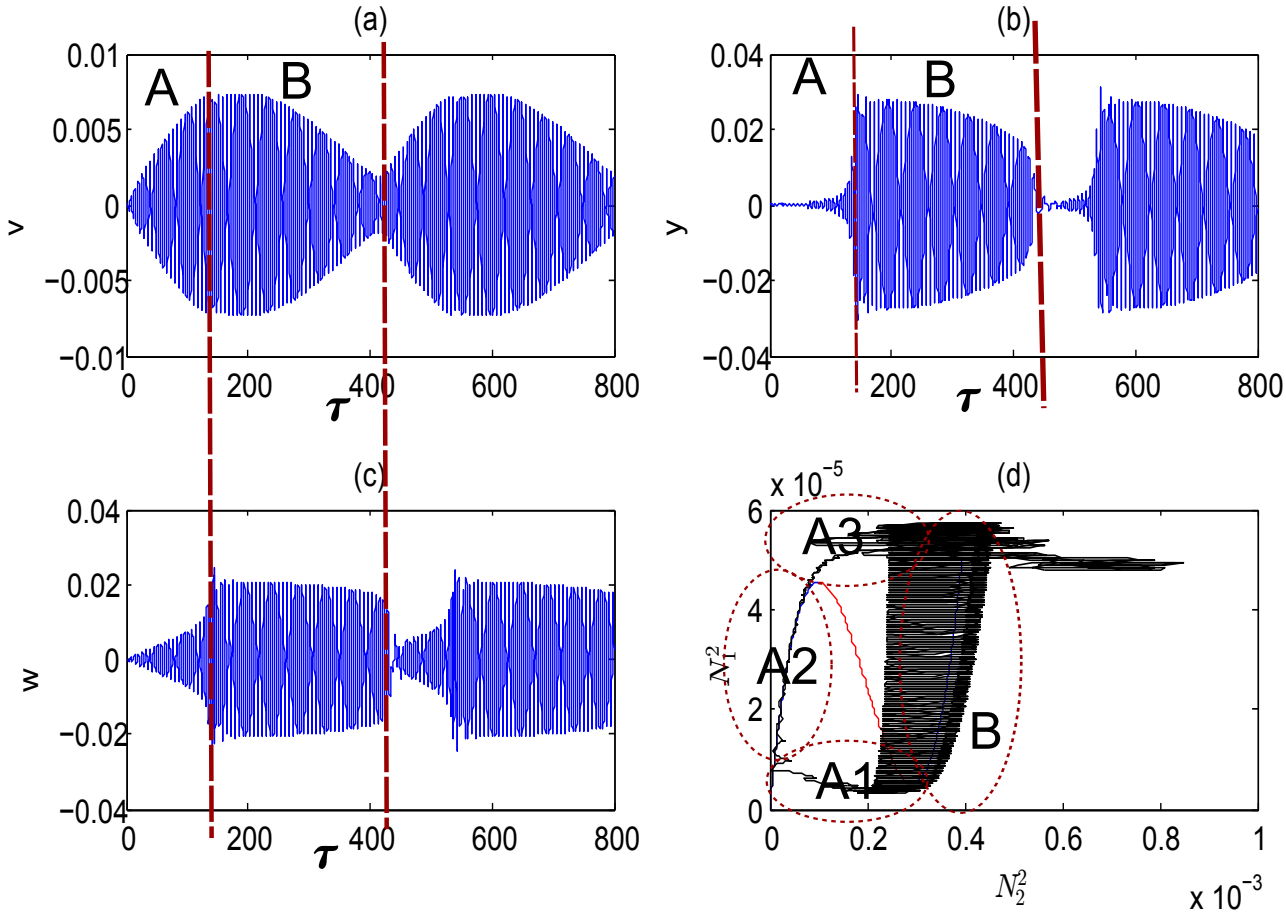

Fig. 7. Cubic NES under periodic forcing with parameters $K = 4500, G = 0.02$ and initial conditions $x_0 = 0, \dot{x_0} = 0, y_0 = 0, \dot{y_0} = 0$. (a) Displacement of the center of gravity. (b) Displacement of cubic NES. (c) Relative displacement between LO and cubic NES. (d) SIM and trace between LO and cubic NES: black curve represents projected motion.

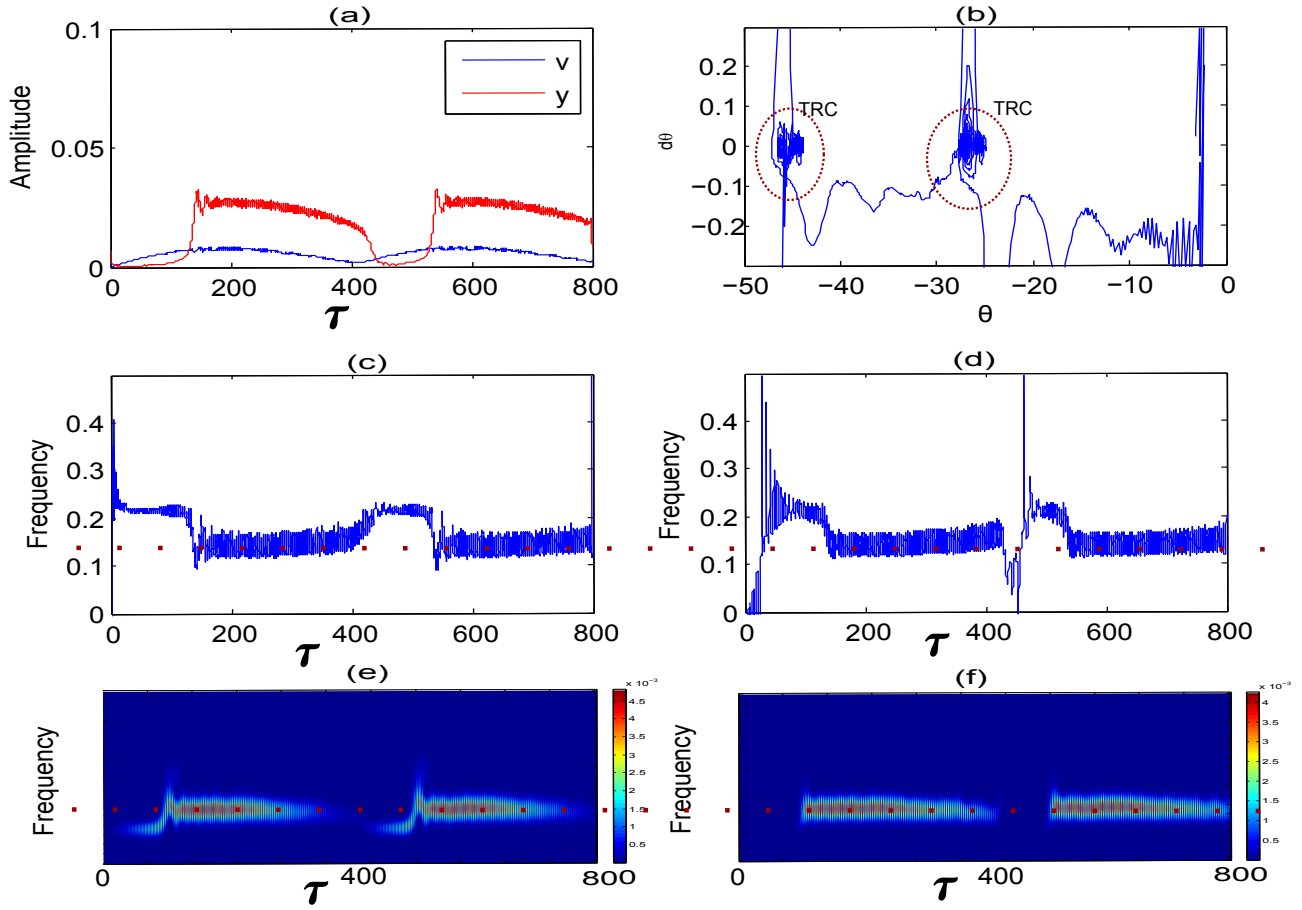

Fig. 8. Cubic NES under periodic forcing with parameters $K = 4500, G = 0.02$ and initial conditions $x_0 = 0, \dot{x_0} = 0, y_0 = 0, \dot{y_0} = 0$. (a) Envelope of v and y. (b) Phase difference between v and y. (c) Instantaneous frequency of v (HT). (d) Instantaneous frequency of y (HT). (e) WT spectrum of v. (f) WT spectrum of y.

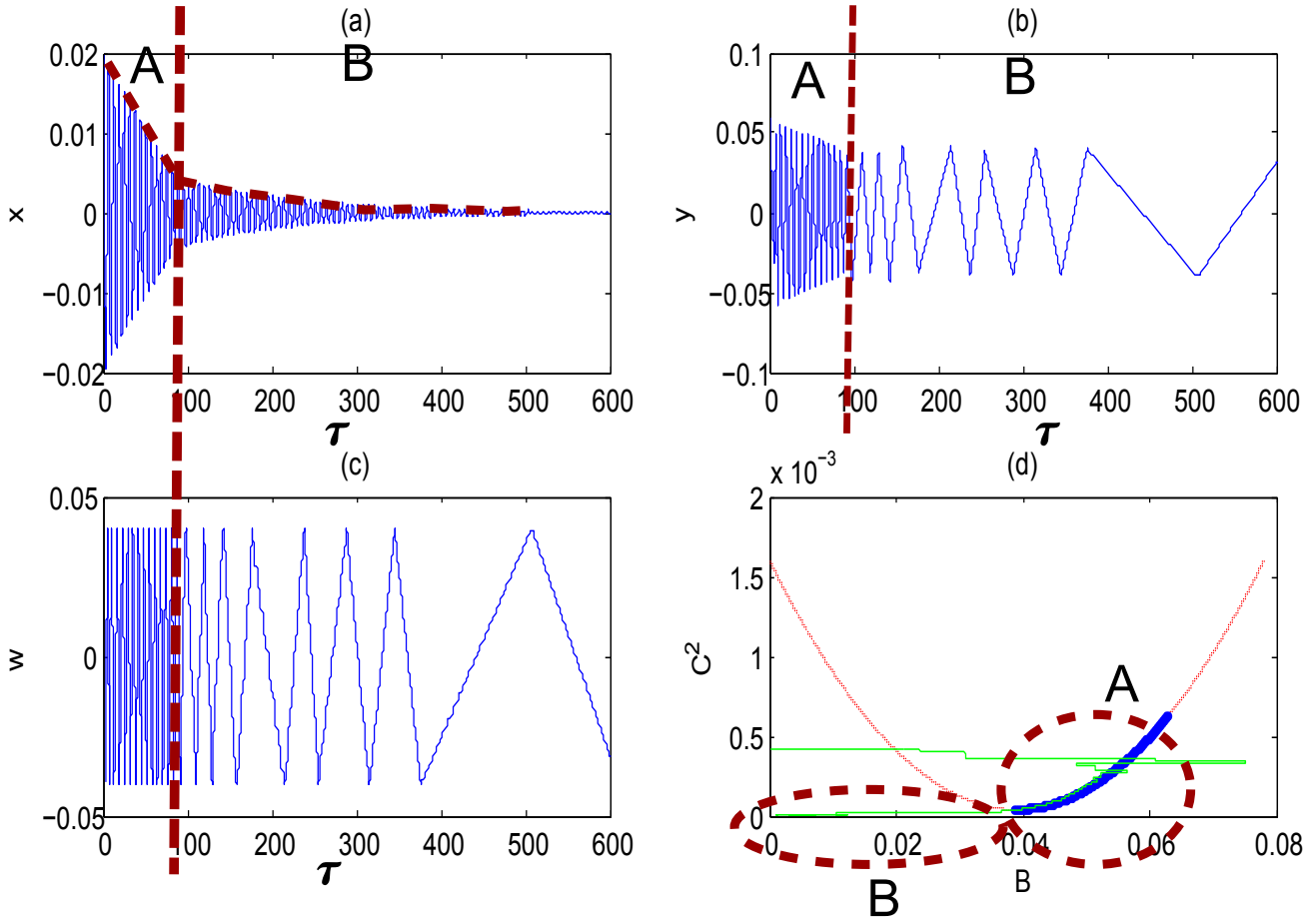

Fig. 9. VI NES under transient forcing with parameters: $B = 0.04, G = 0$ and initial conditions $x_0 = 0.02, \dot{x_0} = 0, y_0 = 0.06, \dot{y_0} = 0$. (a) Displacement of LO. (b) Displacement of VI NES. (c) Relative displacement between LO and VI NES. (d) SIM and trace between LO and VI NES.

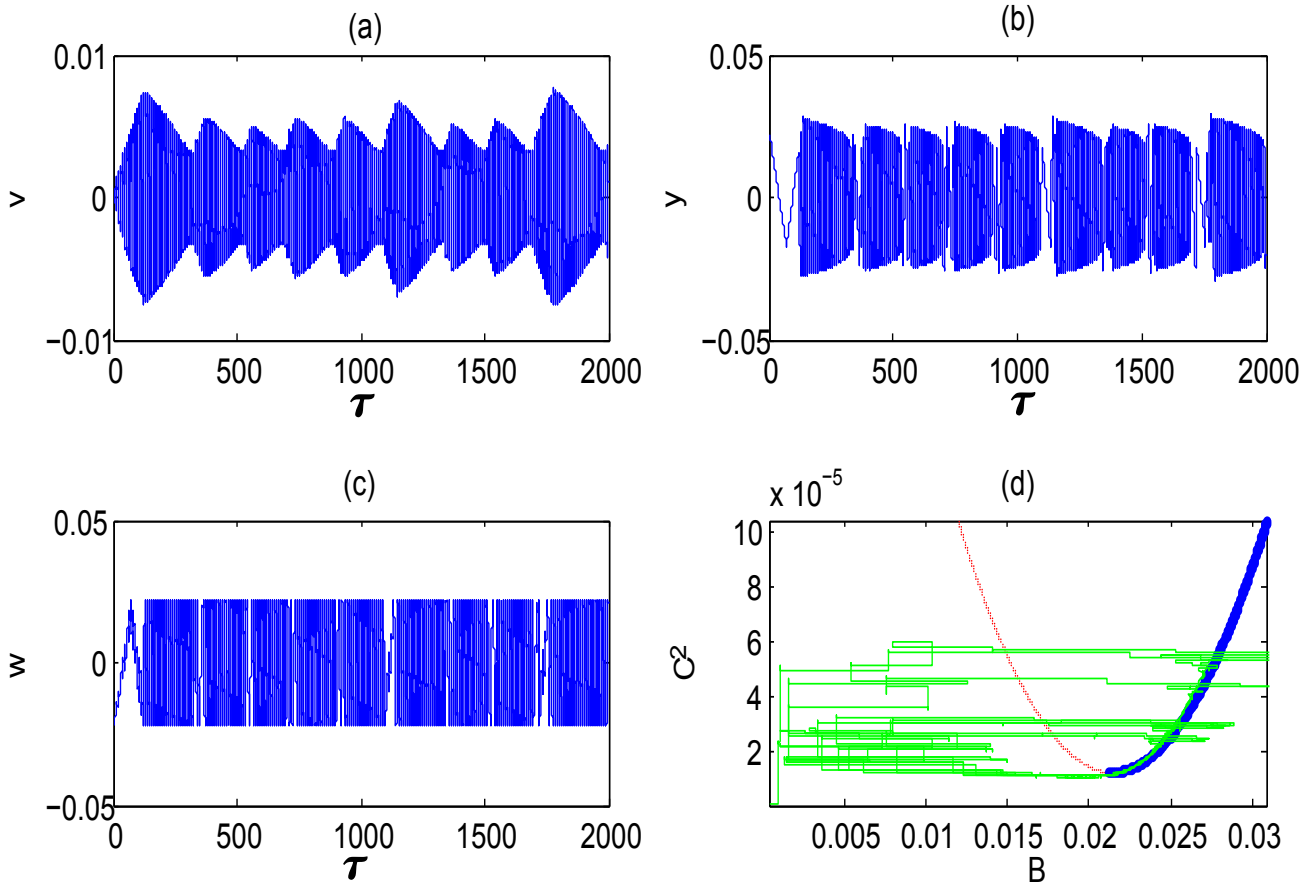

Fig. 10. VI NES under periodic forcing with parameters: $B = 0.04, G = 0$ and initial conditions $x_0 = 0.02, \dot{x_0} = 0, y_0 = 0.06, \dot{y_0} = 0$. (a) Displacement of the center of gravity. (b) Displacement of VI NES. (c) Relative displacement between LO and VI NES. (d) SIM and trace between LO and VI NES.

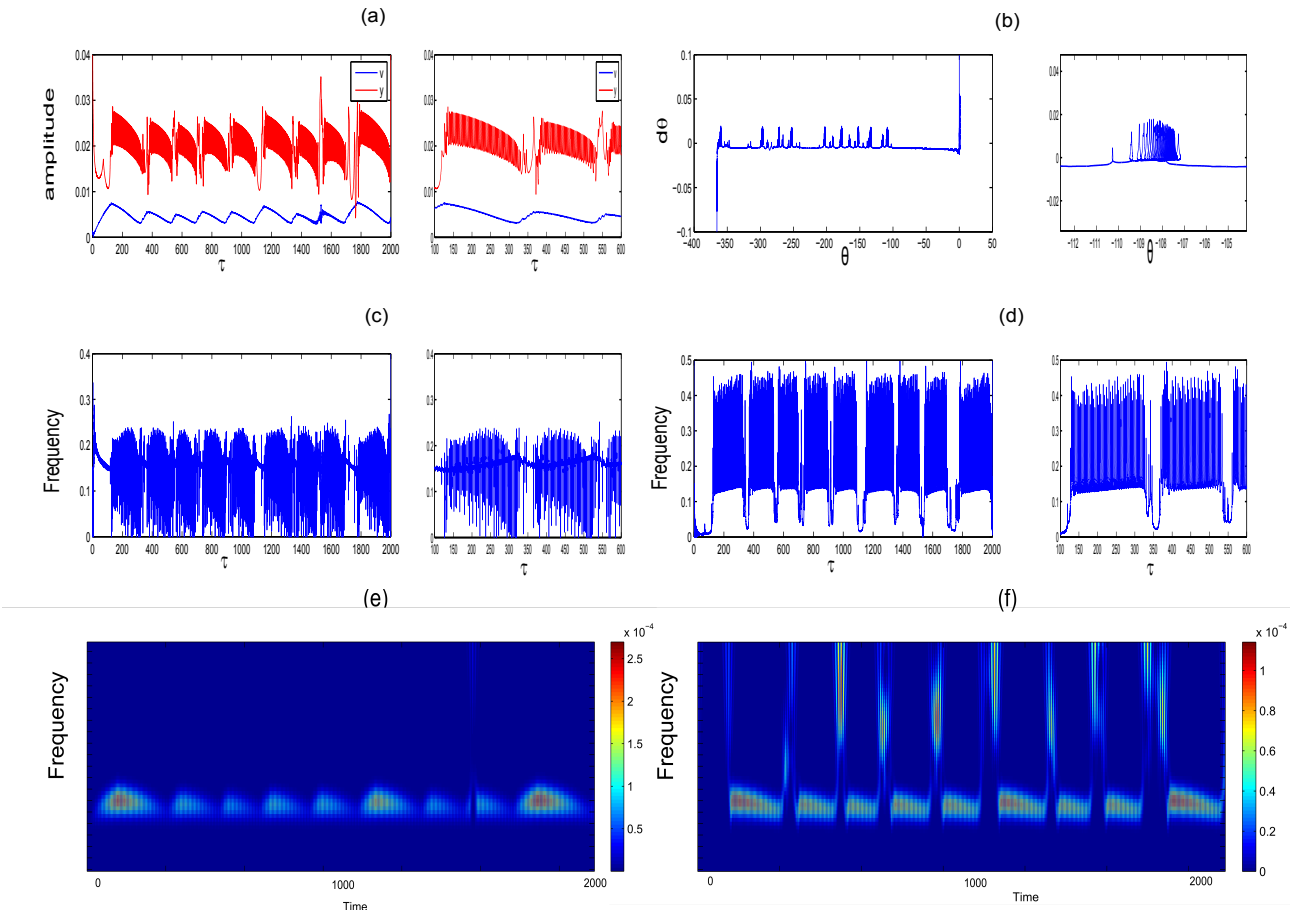

Fig. 11. VI NES under periodic forcing with parameters: $B = 0.04, G = 0, \sigma = 0$ and initial conditions $x_0 = 0.02, \dot{x_0} = 0, y_0 = 0.06, \dot{y_0} = 0$. (a) Envelope of displacement of v and y. (b) Phase difference between v and y. (c) Instantaneous frequency of v (HT). (d)Instantaneous frequency of y (HT). (e) WT spectrum of v. (f) WT spectrum of y.

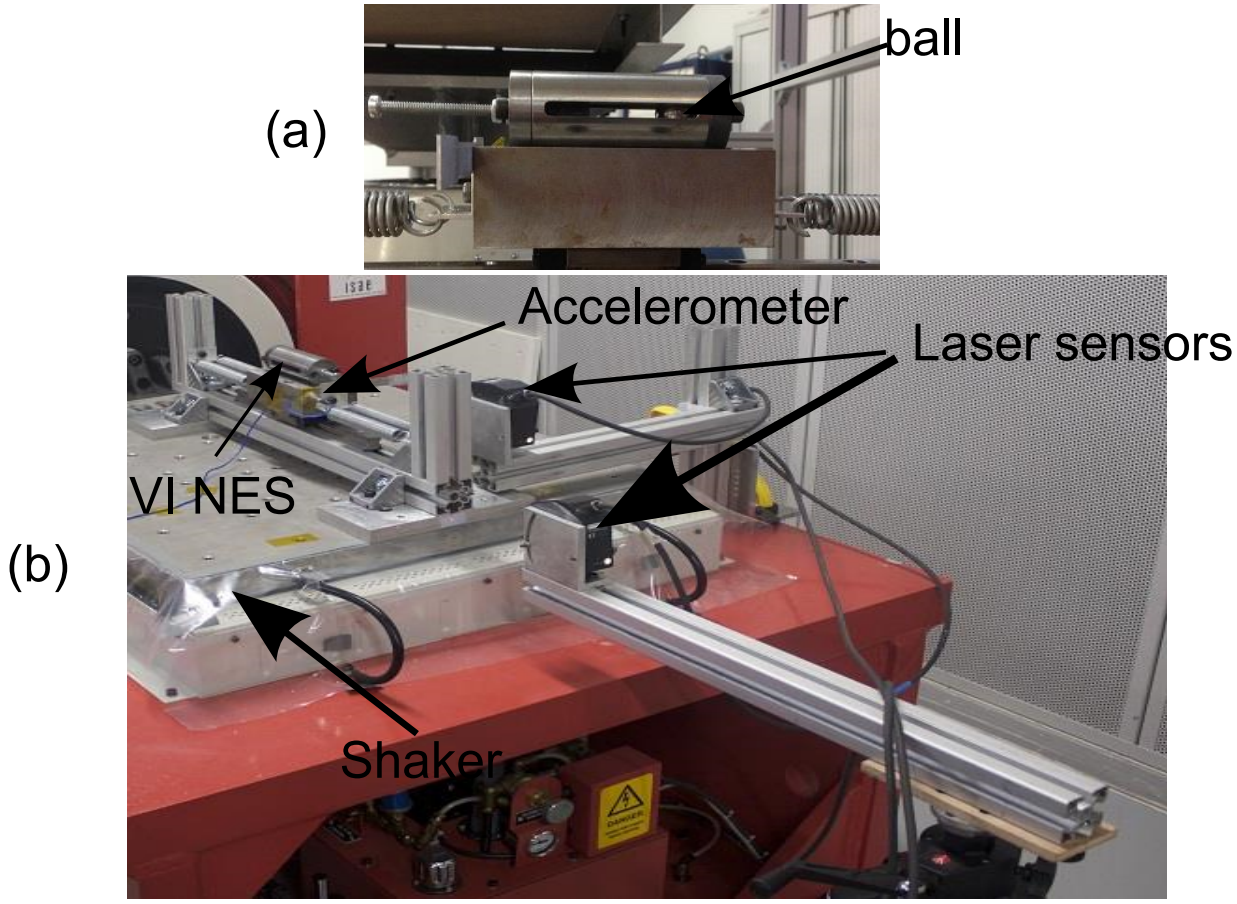

Fig. 12. Picture of the experimental setup: (a) Global view of the system, (b) detailled view of the VI NES.

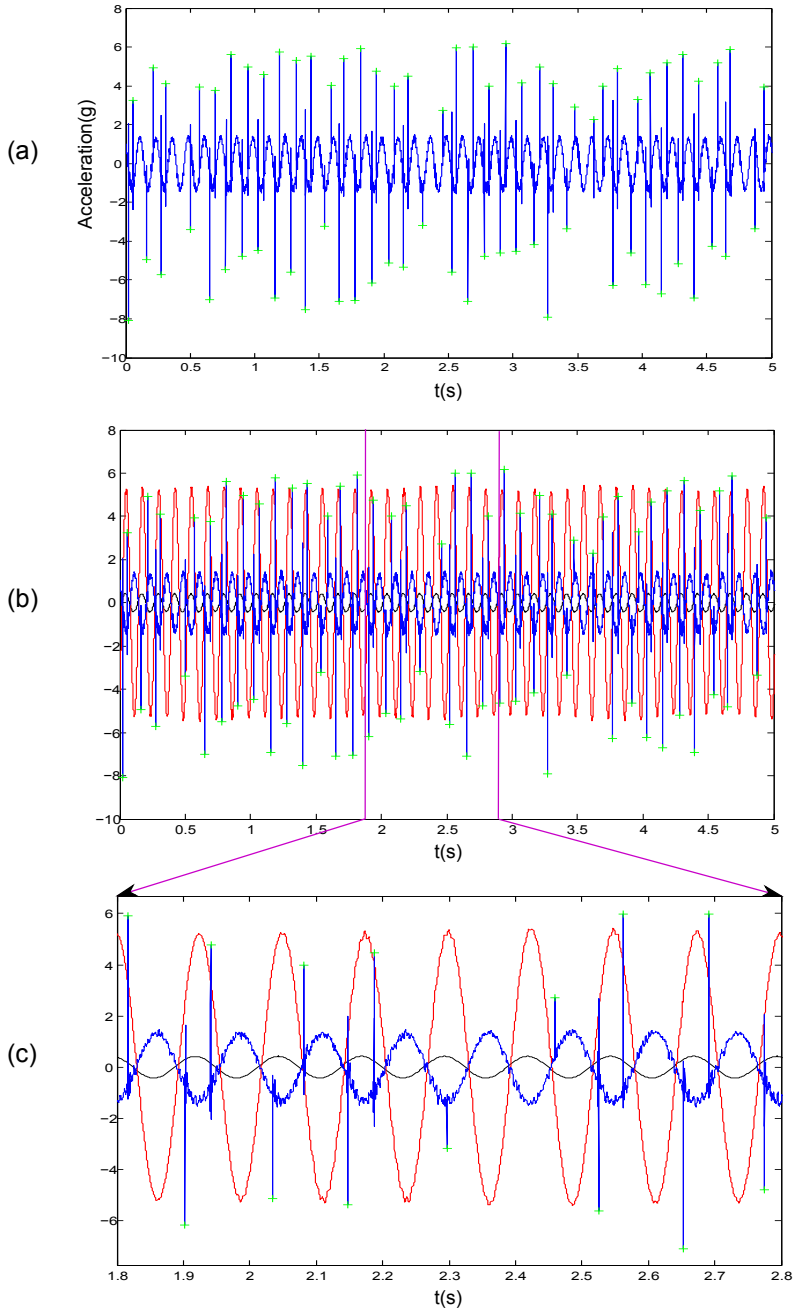

Fig. 13. Case of chaotic SMR: (a) Acceleration of LO. (b) Acceleration of LO in blue line and green cross, displacement (mm) of LO in red line and displacement (mm) of forcing in black line. (c) enlarged view.